Time-domain simulations of sound propagation in a stratified atmosphere over an impedance ground

Benjamin Cotté and Philippe Blanc-Benon
LMFA, UMR CNRS 5509, École Centrale de Lyon, 69134 Ecully Cedex, France
benjamin.cotte@ec-lyon.fr, philippe.blanc-benon@ec-lyon.fr

Abstract: Finite-difference time-domain simulations of broadband sound propagation in a stratified atmosphere are presented. A method recently proposed to obtain an impedance time-domain boundary condition is implemented in a linearized Euler equations solver, which enables to study long range sound propagation over an impedance ground. Some features of the pressure pulse evolution with time are analyzed in both upward-and downward-refracting conditions, and the time-domain simulations are compared to parabolic equation calculations in the frequency domain to show the effectiveness of the proposed impedance boundary condition.

PACS numbers: 43.28.Js, 43.28.En [VO]
Date Received: January 19, 2009 **Date Accepted:** February 18, 2009

1. Introduction

Time-domain numerical solutions of the linearized Euler equations are becoming increasingly popular to study broadband noise propagation outdoors,[1–3] since they can accurately take into account the interactions of the acoustic waves with local wind and temperature fluctuations in the atmospheric boundary layer. They are also well suited to study the sound field close to the acoustic sources, which can be complex in the context of transportation noise.

When performing finite-difference time-domain (FDTD) simulations, one of the main difficulties is to account for the reflection of acoustic waves over an impedance ground. Indeed, impedance models classically used for outdoor grounds have been obtained in the frequency domain, and most of them do not meet the necessary conditions for an impedance model to be physically possible, which means that they cannot be directly translated into the time domain.[4,5] Furthermore, when the translation into the time domain is possible, a convolution needs to be solved in the time-domain boundary condition (TDBC), which is computationally expensive. Different methods have been proposed to derive impedance TDBC.[6–8] Recently, Cotté *et al.*[9] presented a TDBC for the Miki impedance model,[4] which is a physically possible extension of the Delany–Bazley impedance model.[10] This TDBC is based on an approximation of the impedance in the frequency domain, which allows the use of the recursive convolution method,[11] a very efficient technique to calculate a discrete convolution. It can be noticed that another way to account for the interaction of sound waves with an impedance ground is to add an explicit porous layer to the computational domain, as done by Salomons *et al.*[1] and by Van Renterghem and Botteldooren.[2] This method is useful to model certain types of grounds, such as extended-reaction grounds but requires additional calculations to be performed in the porous medium.

In this paper, the method proposed to obtain the impedance TDBC is first summarized. Then, after a brief description of the linearized Euler equations solver, two-dimensional simulations of broadband noise propagation in a stratified atmosphere are presented. The pressure pulses obtained in downward and upward-refracting conditions are compared to the homogeneous case. Finally, the spectra of the time-domain simulations are calculated and compared to parabolic equation simulations in the frequency domain.

2. Derivation of time-domain impedance boundary conditions

Let $p(t)$ be the acoustic pressure and $v(t)$ the component of particle velocity normal to the interface between the ground and the air, with $P(\omega)$ and $V(\omega)$ their respective Fourier transform, t the time, and ω the angular frequency; the $\exp(-j\omega t)$ convention is assumed throughout this paper. Classically, the characteristic impedance $Z(\omega)$ is defined in the frequency domain using $P(\omega)=Z(\omega)V(\omega)$. The direct translation of this boundary condition in the time domain involves a convolution operator that is computationally expensive to solve. Thus, following a method proposed by Fung and Ju[6] and Reymen *et al.*,[7] the characteristic impedance $Z(\omega)$ is approximated as a sum of first-order systems:

$$Z(\omega) \approx \sum_{k=1}^{S} \frac{A_k}{\lambda_k - j\omega}, \tag{1}$$

with λ_k the real poles in the approximation, A_k the corresponding coefficients, and S the number of poles. Using these first-order systems, the impedance is guaranteed to be physically possible if $\lambda_k \geq 0$ and if the passivity condition is met (positive real part of the impedance). Furthermore, the form of these functions allows the use of the recursive convolution method, introduced by Luebbers and Hunsberger[11] in the context of electromagnetic propagation through dispersive media. Considering the discretized variables $p^{(n)}=p(n\Delta t)$ and $v^{(n)}=v(n\Delta t)$, with Δt the time step, the following TDBC is obtained:[9]

$$p^{(n)} = \sum_{k=1}^{S} A_k \phi_k^{(n)}, \tag{2}$$

where the accumulators ϕ_k are given by the recursive formula:

$$\phi_k^{(n)} = v^{(n)} \frac{1 - e^{-\lambda_k \Delta t}}{\lambda_k} + \phi_k^{(n-1)} e^{-\lambda_k \Delta t}. \tag{3}$$

It can be seen that S accumulators ϕ_k are needed in the TDBC, with only two storage locations per accumulator.

Cotté *et al.*[9] compared different methods to identify the coefficients A_k and λ_k of Eq. (1), and showed that it is desirable to constrain the values of the poles λ_k to obtain accurate numerical results. They propose an optimization method in the frequency domain, which guarantees that the impedance model is physically possible and that the values of the poles are sufficiently small. This method is applied to the Miki impedance model of a semi-infinite ground layer:[4]

$$Z/\rho_0 c_0 = 1 + 0.0699(f/\sigma_e)^{-0.632} + j0.107(f/\sigma_e)^{-0.632}, \tag{4}$$

with ρ_0 the air density, c_0 the sound speed in the air, f the frequency, and σ_e an effective flow resistivity [the coefficients in Eq. (4) are in SI units]. The coefficient identification method is performed on the frequency band [50 Hz, 1200 Hz], which includes the spectrum of the pulse used in the simulations presented in Sec. 3. The coefficients A_k and λ_k corresponding to the Miki impedance model with an effective flow resistivity of 100 kPa s m^{-2} are given in Table 1. It can be seen in Fig. 1 that the real and imaginary parts of the impedance are very well approximated using only five real poles over the frequency band of interest. Note that this method has also been applied to the Miki model of a rigidly backed layer in Ref. 9.

3. Time-domain simulations in a stratified atmosphere

3.1 Linearized Euler equation solver

The linearized Euler equations are solved using FDTD methods developed in the computational aeroacoustics community.[12–14] Optimized finite-difference schemes and selective filters over 11 points are used for spatial derivation and grid-to-grid oscillations removal, respectively. These

Table 1. Coefficients A_k and λ_k for the Miki impedance model of a semi-infinite ground layer of effective flow resistivity 100 kPa s m^{-2}. This set of coefficients was referred to as OF v1 in Ref. 9.

k	A_k	λ_k
1	$1.414\,390\,450\,609\times10^{6}$	$5.233\,002\,301\,836\times10^{1}$
2	$1.001\,354\,674\,975\times10^{6}$	$4.946\,064\,975\,401\times10^{2}$
3	$-3.336\,020\,206\,713\times10^{6}$	$1.702\,517\,657\,290\times10^{3}$
4	$5.254\,549\,668\,250\times10^{6}$	$1.832\,727\,486\,745\times10^{3}$
5	$3.031\,704\,943\,714\times10^{7}$	$3.400\,000\,000\,000\times10^{4}$

numerical schemes are optimized in the wave number space by minimizing the dispersion and dissipation errors, so that acoustic wavelengths down to five or six times the spatial mesh size are accurately calculated.[9,15] For the interior points, which are the points separated from the boundary by at least five points, the centered fourth-order finite-difference scheme of Bogey and Bailly[12] and the centered sixth-order selective filter recently proposed by Bogey *et al.*[14] are chosen. For the boundary points, that are the five extreme points in each direction, the 11-point non-centered finite-difference schemes and selective filters of Berland *et al.*[13] are used. Applying a selective filter to a variable U on a uniform mesh of size Δx provides

$$U^f(x_0) = U(x_0) - s_f \sum_{m=-P}^{Q} d_m U(x_0 + m\Delta x). \tag{5}$$

In the following, a filtering coefficient s_f of 0.2 is taken for all selective filters except at the extreme points where a filtering coefficient of $s_f/20$ is chosen. A smaller coefficient is indeed taken for the completely off-centered filter because this filter is much more dissipative than the other selective filters. The completely off-centered filter is needed when a large number of time iterations is performed[15] as it is the case in this paper.

The optimized six-stage Runge–Kutta algorithm of Bogey and Bailly[12] is used for time integration. The TDBC presented in Sec. 2 can easily be adapted to this algorithm, as shown in Ref. 9. The simulations presented in this paper are performed with a CFL$=c_0\Delta t/\Delta x$ of 1, with

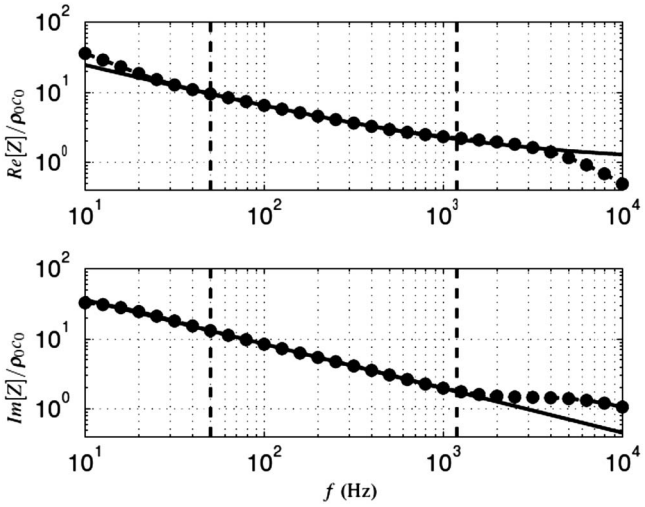

Fig. 1. Real and imaginary parts of the normalized impedance Z/ρ_0c_0. The solid line corresponds to the Miki model of a semi-infinite ground layer with an effective flow resistivity of 100 kPa s m^{-2}, and the dots correspond to the fit obtained using the frequency-domain approximation. The frequency band [50 Hz, 1200 Hz] is represented by vertical lines.

Δt the time step. An orthogonal non-staggered grid is used, and the TDBC given by Eqs. (2) and (3) is only applied at the ground boundary ($z=0$); more details on the numerical implementation of the TDBC can be found in Ref. 9. At all other boundaries, the radiation boundary conditions of Tam and Dong[16] are considered. The initial pressure distribution used in the simulations has the following Gaussian form: $p(r,t=0)=A\exp(-\ln 2r^2/B^2)$, with $B=5\Delta x=0.25$ m the Gaussian half-width, $r=\sqrt{x^2+(z-z_S)^2}$ the source-receiver separation, and $z_S=2$ m the source height. This starter has a broadband spectrum with significant frequency content up to 800 Hz approximately.[9,15]

3.2 Numerical results

In the rest of the paper, a two-dimensional propagation configuration is studied, with a size of approximately 500 m in the x-direction and 100 m in the z-direction. The mesh size is 0.05 m, and there are about 22×10^6 points in the computational domain. The calculation is run over 11 000 time iterations to enable the pulse to leave the computational domain. This calculation is performed on a NEC SX-8 vector machine and takes about 8 h to run (more details can be found in Ref. 15). A logarithmic sound speed profile is considered, which has the following form: $c(z)=c_0+a_c\ln(1+z/z_0)$, with $c_0=340$ m/s and $z_0=0.1$ m. Three values of the coefficient a_c are considered, corresponding to downward-refraction ($a_c=+1$ m/s), upward-refraction ($a_c=-1$ m/s), and homogeneous conditions ($a_c=0$).

Two movies of the pulse evolution with time are given in Mm. 1 for a receiver height of 2 m and Mm. 2 for a receiver height of 10 m. The pressure amplitude is corrected by $\sqrt{r}$ to take into account geometrical spreading in two dimensions. At each distance x, the pressure waveforms are centered at the time x/c_0. The movies show that the pressure pulse arrives earlier in the downward-refracting case ($a_c=+1$ m/s) and later in the upward-refracting case ($a_c=-1$ m/s) compared to the homogeneous case ($a_c=0$). There is evidence of multiple arrivals in the downward-refracting case, with relatively strong acoustic pressure amplitude. In the upward-refracting case, the pulse amplitude is attenuated compared to the homogeneous case, except at short range where an amplification of the acoustic pressure can be observed. This amplification can be attributed to a modification of the ground effect due to the vertical sound speed gradients close to the ground. This effect is particularly clear for a receiver height of 10 m and distances between 50 and 100 m approximately in Mm. 2, and the modification of the ground effect will appear on the spectra plotted in Fig. 3. Another feature of the pressure waveforms shown in the movies is the presence of a long trail at the end of the pulses. This long trail component has been shown to be a surface wave in Ref. 17. It must be noted that in the atmosphere, the insonification of the refractive shadow zone is mainly caused by sound scattering by turbulence; however, this effect is not considered in this paper.

Mm. 1. Normalized pressure $p(t)\sqrt{r}/A$ with respect to time at a height of 2 m and distances between 10 and 500 m. The blue curve corresponds to the downward-refracting case ($a_c=+1$ m/s), the black curve to the homogeneous case ($a_c=0$), and the red curve to the upward-refracting case ($a_c=-1$ m/s). This a file of type "avi" (3.7 Mbytes).

Mm. 2. The same as in Mm. 1, but for a height of 10 m. This a file of type "avi" (3.9 Mbytes).

4. Comparison with parabolic equation simulations in the frequency domain

The time-domain simulations are now compared to parabolic equation (PE) calculations in the frequency domain to show the effectiveness of the impedance TDBC described in Sec. 2. The spectra of the sound pressure level relative to the free field, noted ΔL, are calculated using a fast Fourier transform. The PE calculations are obtained using a wide-angle parabolic equation (WAPE) code described in Refs. 18 and 15, with a frequency-domain impedance boundary condition based on Eq. (4). The spectra of ΔL for the FDTD and PE calculations are compared in Fig. 2 for a receiver height of 2 m, and in Fig. 3 for a receiver height of 10 m. Both solutions agree very well between 50 and 800 Hz. Above 800 Hz, there is no significant energy in the

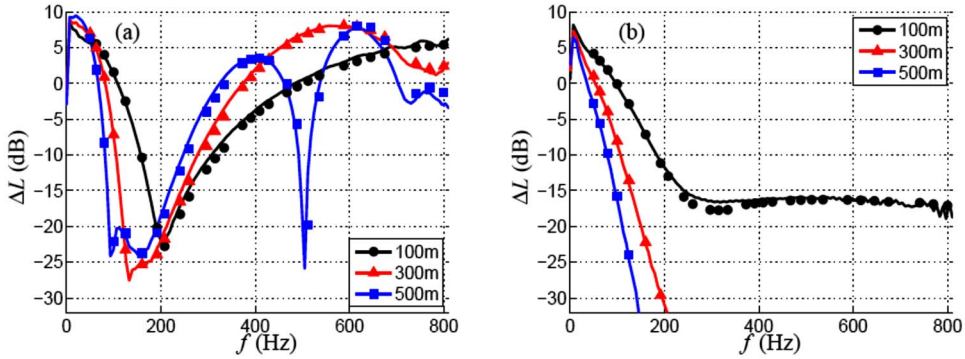

Fig. 2. (Color online) Spectra of the sound pressure level relative to the free field ΔL at a height of 2 m and propagation distances of 100, 300, and 500 m (a) in downward-refracting conditions ($a_c = +1$ m/s) and (b) in upward-refracting conditions ($a_c = -1$ m/s). The solid lines correspond to the FDTD calculations, and the symbols correspond to the PE calculations.

initial pulse of the FDTD calculation. Propagation distances are thus greater than 1000 acoustic wavelengths for the largest range and frequency considered in these simulations, which shows that the proposed FDTD model is well suited to study long range sound propagation.

These spectra also explain the pressure pulse evolution with time shown in Mm. 1 and Mm. 2. In downward-refracting conditions [see Figs. 2(a) and 3(a)], the sound pressure levels are quite large and the interference pattern is complex, especially at a range of 500 m, which can be linked to the multiple arrivals that are observed in the movies. In upward-refracting conditions [see Figs. 2(b) and 3(b)], the frequency components above 200 Hz are strongly attenuated at ranges greater or equal to 300 m. Thus, the pressure pulse contains only very low-frequency components at these ranges. At a receiver height of 10 m and a range of 100 m, however, the sound pressure level is quite large over the whole frequency band of interest, and even larger than the sound pressure level in downward-refracting conditions. The interference dip located at about 200 Hz in the downward-refracting case is shifted to higher frequencies in the upward-refracting case, which explains the pulse amplification observed in the movie Mm. 2.

5. Conclusion

In this paper, long range sound propagation over an impedance ground is studied using FDTD methods. In particular, a method recently proposed to obtain an impedance TDBC has been applied to the Miki impedance model. This TDBC has been implemented in a linearized Euler

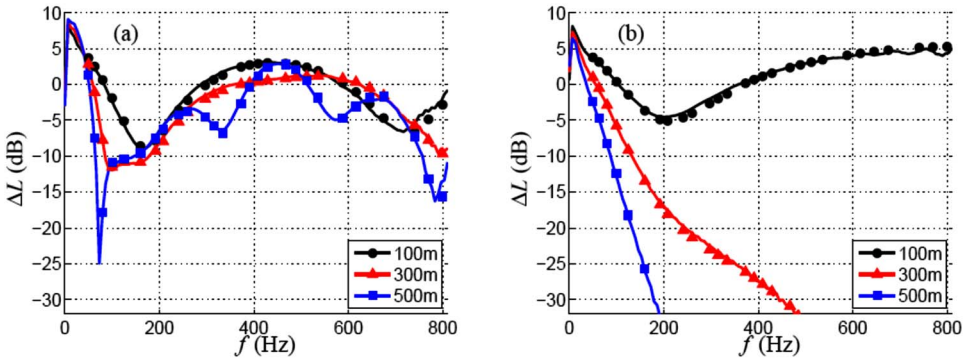

Fig. 3. (Color online) The same as in Fig. 2, but for a height of 10 m.

equations solver and two-dimensional simulations in a stratified atmosphere have been presented. One type of ground has been tested in the simulations on the frequency range [50 Hz, 800 Hz]. The solver used in this work enables to study sound propagation over distances greater than 1000 acoustic wavelengths, as the comparison with PE calculations in the frequency domain has shown. Interesting features of the pressure pulse evolution with time in both upward- and downward-refracting conditions have been analyzed. In the future, the surface wave component that appears in the time-domain solution will be studied in more detail.

Acknowledgments

Support by CNRS and SNCF is gratefully acknowledged. Computing time was supplied by the Institut du Développement et des Ressources en Informatique Scientifique, Centre National de la Recherche Scientifique. The authors would like to thank the reviewers for their constructive comments and suggestions.

References and links

[1]E. M. Salomons, R. Blumrich, and D. Heimann, "Eulerian time-domain model for sound propagation over a finite-impedance ground surface. Comparison with frequency-domain models," Acta. Acust. Acust. **88**, 483–492 (2002).
[2]T. Van Renterghem and D. Botteldooren, "Numerical simulation of the effect of trees on downwind noise barrier performance," Acta. Acust. Acust. **89**, 764–778 (2003).
[3]D. K. Wilson, S. L. Collier, V. E. Ostashev, D. F. Aldridge, N. P. Symons, and D. H. Marlin, "Time-domain modeling of the acoustic impedance of porous surface," Acta. Acust. Acust. **92**, 965–975 (2006).
[4]Y. Miki, "Acoustical properties of porous materials—Modifications of Delany-Bazley models," J. Acoust. Soc. Jpn. **11**, 19–24 (1990).
[5]Y. H. Berthelot, "Surface acoustic impedance and causality," J. Acoust. Soc. Am. **109**, 1736–1739 (2001).
[6]K.-Y. Fung and H. Ju, "Broadband time-domain impedance models," AIAA J. **39**, 1449–1454 (2001).
[7]Y. Reymen, M. Baelmans, and W. Desmet, "Time-domain impedance formulation suited for broadband simulations," in 13th AIAA/CEAS Aeroacoustics Conference, Rome, Italy, (2007), AIAA Paper No. 2007-3519.
[8]V. E. Ostashev, S. L. Collier, D. K. Wilson, D. F. Aldridge, N. P. Symons, and D. Marlin, "Padé approximation in time-domain boundary conditions of porous surfaces," J. Acoust. Soc. Am. **122**, 107–112 (2007).
[9]B. Cotté, P. Blanc-Benon, C. Bogey, and F. Poisson, "Time-domain impedance boundary conditions for simulations of outdoor sound propagation," AIAA J. (in press). See also AIAA Paper 2008-3021.
[10]M. E. Delany and E. N. Bazley, "Acoustical properties of fibrous absorbent materials," Appl. Acoust. **3**, 105–116 (1970).
[11]R. J. Luebbers and F. Hunsberger, "FDTD for Nth-order dispersive media," IEEE Trans. Antennas Propag. **40**, 1297–1301 (1992).
[12]C. Bogey and C. Bailly, "A family of low dispersive and low dissipative explicit schemes for flow and noise computations," J. Comput. Phys. **194**, 194–214 (2004).
[13]J. Berland, C. Bogey, O. Marsden, and C. Bailly, "High order, low dispersive and low dissipative explicit schemes for multiple-scale and boundary problems," J. Comput. Phys. **224**, 637–662 (2007).
[14]C. Bogey, N. Cacqueray, and C. Bailly, "A shock-capturing methodology based on adaptative spatial filtering for high-order non-linear computations," J. Comput. Phys. **228**, 1447–1465 (2009).
[15]B. Cotté, "Propagation acoustique en milieu extérieur complexe: Problèmes spécifiques au ferroviaire dans le contexte des trains à grande vitesse (Outdoor sound propagation in complex environments: Specific problems in the context of high speed trains)," Ph.D. thesis 2008-19, École Centrale de Lyon, Ecully Cedex (2008).
[16]C. K. W. Tam and Z. Dong, "Radiation and outflow boundary conditions for direct computation of acoustic and flow disturbances in a nonuniform mean flow," J. Comput. Acoust. **4**, 175–201 (1996).
[17]B. Cotté and P. Blanc-Benon, "Outdoor sound propagation simulations in the time domain using linearized Euler equations with suitable impedance boundary conditions," in Proceedings of the 13th International Symposium on Long Range Sound Propagation, Lyon, France, (2008).
[18]B. Cotté and P. Blanc-Benon, "Estimates of the relevant turbulent scales for acoustic propagation in an upward refracting atmosphere," Acta. Acust. Acust. **93**, 944–958 (2007).